Layout Optimization of the Beam Spot Locations Scanned by Electromagnets in Particle Beam Therapy

AUTHOR(S):

SAKAMOTO, Yusuke; NAGASHIMA, Takayuki; SATO, Yuki; IZUI, Kazuhiro; NISHIWAKI, Shinji

CITATION:

SAKAMOTO, Yusuke ...[et al]. Layout Optimization of the Beam Spot Locations Scanned by Electromagnets in Particle Beam Therapy. Mechanical Engineering Journal 2022, 9(5): 22-00140.

ISSUE DATE:

2022

URL:

http://hdl.handle.net/2433/284481

Bulletin of the JSME Vol.9, No.5, 2022
Mechanical Engineering Journal

Layout optimization of the beam spot locations scanned by electromagnets in particle beam therapy

Yusuke SAKAMOTO*, Takayuki NAGASHIMA*, Yuki SATO*, Kazuhiro IZUI* and Shinji NISHIWAKI*
* Department of Mechanical Engineering and Science, Kyoto University
Kyotodaigaku-katsura C3, Nishikyo-ku, Kyoto 615-8540, Japan
E-mail: sakamoto.yusuke.85c@kyoto-u.jp

Received: 3 April 2022; Revised: 24 July 2022; Accepted: 8 September 2022

Abstract
This paper presents a layout optimization method of the spot locations of pencil beam scanning for particle beam cancer therapy. With the pencil beam scanning technique, the particle beam is scanned from spot to spot in the tumor by using scanning magnets. To provide clinically ideal dose distributions and less-invasive treatment to the patients, both the spot locations and the number of particles given to each spot should be optimized. However, the spot layout is fixed with a lattice pattern in many prior studies. We propose the optimization method to derive the non-lattice spot layout to realize an acceptable dose distribution with a reduced number of spots. With the proposed method, a large enough number of spots were located densely at the initial state, and then the spots with the smallest contribution were removed one by one through iterations. The number of particles given to each spot was determined by solving a quadratic problem. Furthermore, we also propose the idea to accelerate the optimization process by simultaneously removing multiple spots. The algorithm was confirmed by numerical examples of both two-dimensional and three-dimensional cases. The dose quality with the optimized spot layout was better than that with the conventional lattice spot patterns, with all tested cases. In the optimized spot layout, the spots were located on the closed lines which were concentric to the target contour. We also confirmed the proposed method of multiple-remotion can accelerate the optimization process without violating the dose quality.

Keywords : Layout optimization, Heuristic approach, Three-dimensional locations, Scanning magnet, Particle beam therapy

1. Introduction

Particle beam therapy (Loeffler et al., 2013; Kraft, 2000) has attracted increasing interest as a less-invasive cancer treatment compared with other therapies such as surgery, chemotherapy or X-ray radiotherapy. When the charged particles such as protons or carbon ions with high energy are irradiated into the patient, the kinetic energy of the particles is transferred to the body through the ionization effect and the cells in the cancer tumor are destroyed. The radiation dose, which is the energy absorption from the particle beam, becomes maximum at the certain depth from the patient skin where the particles stop in the patient's body. This feature of the dose distribution in the depth direction is called the Bragg peak, and the peak depth can be controlled by changing the initial beam energy. To generate a high energy particle beam, a particle accelerator such as a cyclotron or synchrotron is used. After acceleration, the particle beam is administered to the patient in the treatment room.

For the clinical purpose, the dose should be as ideally homogeneous within the tumor and simultaneously as low outside the tumor as possible. The pencil beam scanning (PBS) technique is currently a very popular irradiation method to form a three dimensional dose distribution which precisely matches the target shape (Kanai et al., 1983; Pedroni et al., 1995). With PBS, many beam irradiation points, which are called spots, are located in the patient's body and a particle beam is administered to each spot. After the dose is given to one spot, the beam is moved to the next spot. The beam sequentially irradiates all the spots which are arranged inside and around the target volume, as if painting it out by a pencil. The beam motion is controlled by the magnetic field generated by a pair of electromagnets called scanning magnets (Miao

Paper No.22-00140
J-STAGE Advance Publication date : 17 September, 2022
[DOI: 10.1299/mej.22-00140]

et al., 2017) which are installed in the beam irradiation nozzle. In order to determine the operation pattern of the scanning magnets, both the positions of all the spots and the number of particles given to each spot must be determined by using the optimization technique.

In many prior studies in PBS, the positions of the beam irradiating spots are set to be basically lattice patterns and are unchanged through optimization, although the number of particles to each spot is optimized to form an ideal dose distribution (Kramer et al., 2000). In addition, shortening the treatment time is also an important criteria for the physical burden of the patient, and decreasing the number of spots directly contributes to the treatment time reduction. By using heuristic approaches such as simulated annealing, several researchers addressed proposing the scan path optimization technique to find the best order of spots to be irradiated for minimizing the total path length of the beam motion (Kang et al., 2007; Wu et al., 2019). In these studies, however, the spot positions were still fixed with the lattice pattern and the number of spots was also fixed.

The contour scanning technique (Meier et al., 2017) was proposed as a non-lattice spot layout, in which spots are located on the contour of the target and its concentric curves. In this method, however, the spot positions were determined on a rule-base and the mathematical optimality of the spot layout was not discussed.

On the other hand, in the research field of mechanical engineering, many position optimization techniques were studied for various purposes.

Fukushima et al. (2004) proposed an optimization method of engine mounting layout in a vehicle, using the Most Probable Optimum Design (MPOD) method. Similarly, Nishiura et al. (2015) proposed an optimization of the stator pole arrangement of a spherical actuator by a genetic algorithm. In these methods, the locations of multiple objects were optimized while the number of the objects never changed through optimization. Matsumoto et al. (2021) proposed a method to determine the optimal placement of solar arrays that maximize the total amount of received light. With this method, the layout of the solar arrays was kept to a lattice pattern while the number of solar arrays was optimized by changing the interval of the solar arrays and the relative position of the lattice coordinate to the site boundary.

On the other hand, Yamaki et al. (2018) proposed an actuator layout design method for deformable mirrors in fundus imaging modality. Their method can obtain the optimal layout of a minimum number of actuators while keeping the error of mirror surface deformation small enough. In their approach, many actuators were located at the initial step and then an actuator was removed step by step based on the contribution of each actuator.

In this research, we construct a heuristic method in determining optimum spot locations in PBS, which can realize acceptable dose distribution with a smaller number of spots than the conventional lattice pattern. First, we formulate the dose optimization problem with fixed spot locations. Then we present the algorithm to obtain optimum spot locations by iteratively removing the spot with low contribution to form the dose distribution. Unlike the method of Yamaki et al. which optimizes the two-dimensional locations of several tens of actuators, the spots in PBS are located in three-dimensions, and usually more than thousands of spots should be removed. We also propose the improved method to accelerate the optimization process by introducing a multiple spot reduction scheme and confirm its effectiveness.

2. Methods

2.1. Pencil beam scanning overview

Figure 1 shows a schematic of PBS. The target volume is divided into plural layers which are perpendicular to the beam direction and spots are located in each layer. Each spot in the layer is sequentially irradiated, as it is painted by a moving pencil beam. After every spot in one layer is irradiated, the beam energy is shifted to change the layer. Here, we define the coordinate in which the beam direction is along the z axis and the layers are parallel to the xy plane. The spots are located mainly inside the target T. A small number of spots are also located outside and close to the target boundary, in order to enhance the dose sharpness at the target edge.

Figure 2 (a) shows a schematic of the irradiation nozzle for PBS. A pair of scanning magnets are installed in the nozzle and each of them generates a magnetic field to the y and x directions. Since the particle beam is a positive charge, the beam direction is slightly bent to the x and y directions by the Lorentz force. The xy position of the beam at the patient can be controlled by adjusting the current to the scanning magnet which correlates to the strength of the magnetic field and the beam bending angle. The nozzle also contains the beam position monitor and the dose monitor which enable the feedback control of the beam position and the beam dose, respectively. Figure 2 (b) shows an example of the operation pattern of the scanning magnets and Fig. 2 (c) shows the path of the beam position in the xy plane. The beam position stays at a spot when the magnetic fields of both magnets are fixed, and the beam position moves to the x or y direction when the corresponding magnetic field changes. The time length of staying at a spot corresponds to the number of particles to

[DOI: 10.1299/mej.22-00140]

be irradiated to the spot.

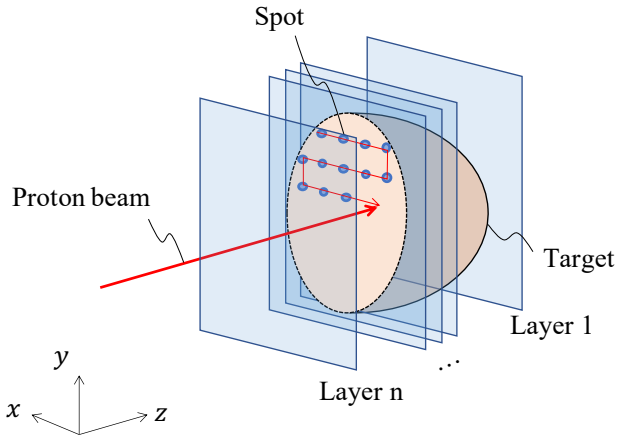

Fig. 1 Image of the beam spots in PBS.

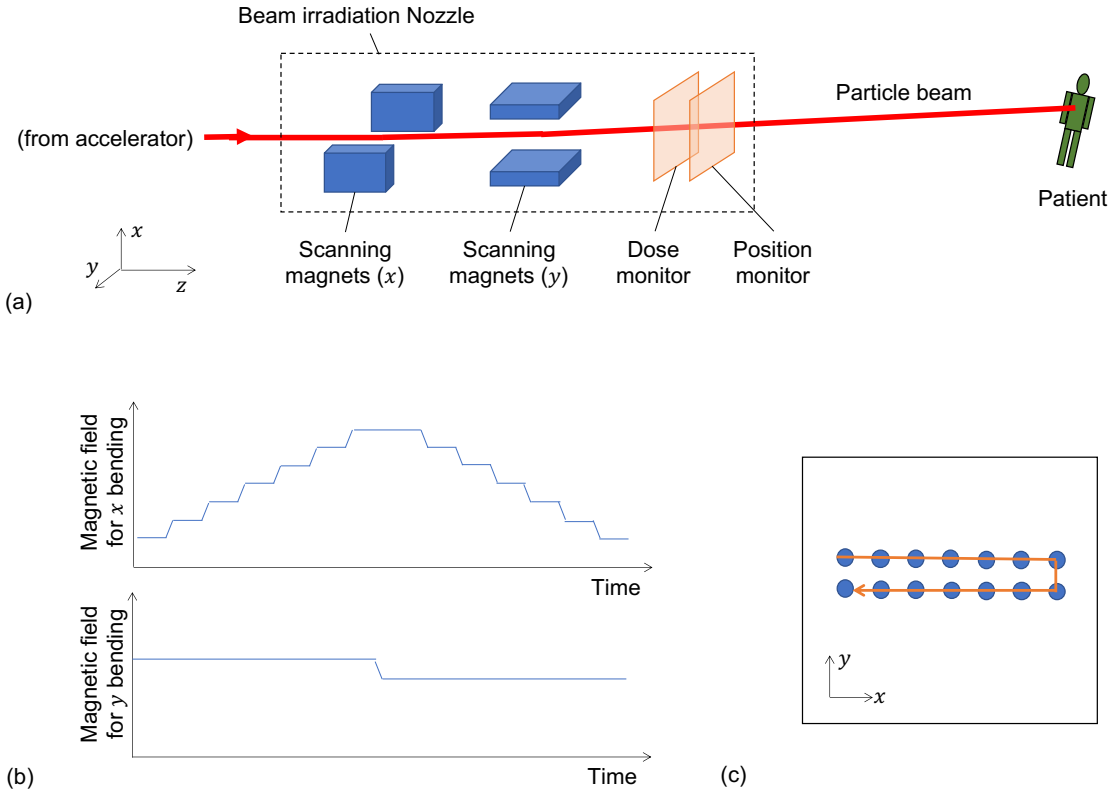

Fig. 2 (a) Schematic of the beam irradiation nozzle and the scanning magnets in PBS. (b) Example of the scanning magnet operation. (c) Example of the beam position motion corresponding to the scanning magnet operation in (b).

2.2. Formulation of dose distribution calculation

We assumed the two-dimensional Gaussian as the dose distribution of a single spot in the xy plane, as follows.

$$D_{xy:i}(x,y) = \frac{1}{2\pi\sigma^2}\exp\left(-\frac{(x-x_i)^2+(y-y_i)^2}{2\sigma^2}\right), \tag{1}$$

where (x_i, y_i) denotes the position of the i-th spot, and σ is the beam spot size. Here, we consider the spot shape is approximately isotropic, while the actual beam spot shape is an ellipsoid represented by using σ_x and σ_y.

[DOI: 10.1299/mej.22-00140]

Depth dose distribution along the z direction is obtained by Monte-Carlo simulation (Akagi et al., 2014).

Figure 3 shows the simulated depth dose distribution $D_{z:i}(z)$ of proton beam with the energy of 130 MeV. Three-dimensional dose distribution of a single spot is calculated by the multiplication of two-dimensional dose and depth dose distribution as

$$D_i(x, y, z) = D_{xy:i}(x, y) \times D_{z:i}(z). \tag{2}$$

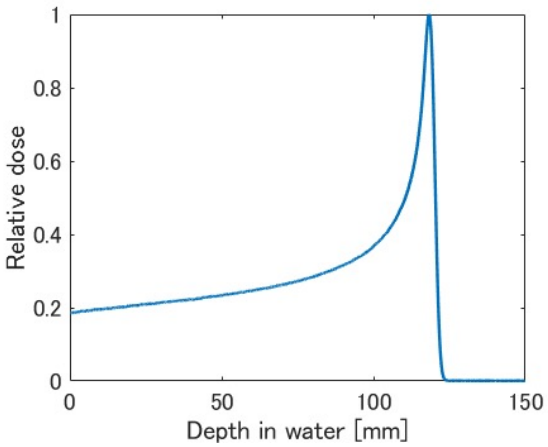

Fig. 3 Simulated depth dose distribution of the particle beam.

The total dose distribution D_{total} is calculated as the weighted sum of contribution from each spot as

$$D_{total}(x, y, z) = \sum_{i=1}^{N} \chi_i D_i(x, y, z), \tag{3}$$

where χ_i stands for the number of particles delivered to the i-th spot and N stands for the number of spots.

2.3. Requirements for the dose distribution

In particle beam therapy, the dose distribution is required to be homogeneous inside the target while it should be as small as possible outside the target. In this study, we set the objective function f as follows.

$$f = w_1 f_1 + w_2 f_2 + w_3 f_3. \tag{4}$$

$$f_1 = \frac{\int_T \left(D_{total}(x, y, z) - D_{obj}\right)^2 d\Omega}{\int_T d\Omega}. \tag{5}$$

$$f_2 = \frac{\int_{\bar{T}} (D_{total}(x, y, z))^2 d\Omega}{\int_{\bar{T}} d\Omega}. \tag{6}$$

$$f_3 = \frac{\int_O (D_{total}(x, y, z))^2 d\Omega}{\int_O d\Omega}. \tag{7}$$

Here, f_1, and f_2 stand for the square of the dose difference from the objective dose D_{obj} in the target region, T, and the square dose in the region outside the target, $\bar{T}$, respectively. Besides, particularly important organs where it is strongly desired to avoid the dose irradiation, such as the heart or the esophagus, are called as organs at risk (OARs) and f_3 stands for the square of the dose in the OAR region, O. Figure 4 shows a general, simple schematic of the regions T, $\bar{T}$, and O. The symbols w_1, w_2, and w_3 are the weighting factors for f_1, f_2, and f_3, respectively. Each of f_1, f_2, and f_3 is normalized by the total volume of the region. In this objective function, the first term f_1 makes the dose distribution close to the ideal one inside the target. The second term f_2 and the third term f_3 reduce the total amount of unnecessary dose outside the target and in the OAR, respectively. The region O is usually included in $\bar{T}$ and w_3 is set to be a larger value than w_2 to reduce the OAR dose more strongly than the dose at general volume outside the target.

[DOI: 10.1299/mej.22-00140]

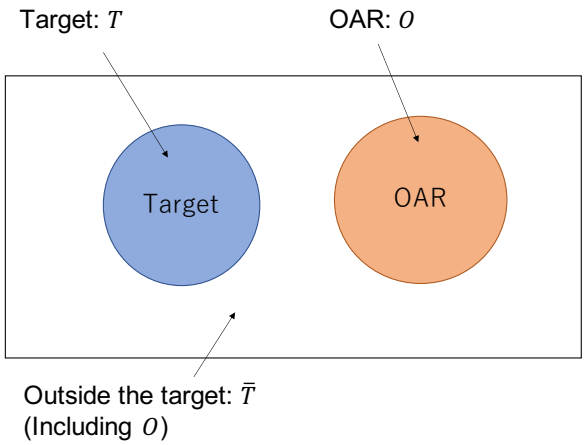

Fig. 4 Relationship among the target, outside the target, and the OAR

2.4. Particle number optimization with a fixed spot layout

The objective functions in Eqs. (4-7) can be transformed as follows. The integration in the target T is calculated as

$$\begin{aligned}\int_T \left(D_{total} - D_{obj}\right)^2 d\Omega &= \int_T \left(\sum_{i=1}^{N} \chi_i D_i - D_{obj}\right)^2 d\Omega \\ &= \int_T \left(\sum_{i=1}^{N}\sum_{j=1}^{N} \chi_i\chi_j D_i D_j - 2D_{obj}\sum_{i=1}^{N}\chi_i D_i + {D_{obj}}^2\right) d\Omega \\ &= \sum_{i=1}^{N}\sum_{j=1}^{N} \chi_i\chi_j \int_T D_i D_j d\Omega - 2D_{obj}\sum_{i=1}^{N}\chi_i \int_T D_i d\Omega + {D_{obj}}^2 \int_T d\Omega. \end{aligned} \tag{8}$$

The integration outside the target $\bar{T}$ is calculated as

$$\begin{aligned}\int_{\bar{T}} \left(D_{total}\right)^2 d\Omega &= \int_{\bar{T}} \left(\sum_{i=1}^{N} \chi_i D_i\right)^2 d\Omega \\ &= \int_{\bar{T}} \sum_{i=1}^{N}\sum_{j=1}^{N} \chi_i\chi_j D_i D_j d\Omega \\ &= \sum_{i=1}^{N}\sum_{j=1}^{N} \chi_i\chi_j \int_{\bar{T}} D_i D_j d\Omega. \end{aligned} \tag{9}$$

The integration in the OAR O is also calculated the same as Eq. (9). Therefore, the objective function f is represented as

$$f = \boldsymbol{X}^T \boldsymbol{H} \boldsymbol{X} + D_{obj}\boldsymbol{\Lambda}^T \boldsymbol{X} + {D_{obj}}^2, \tag{10}$$

where the matrix $\boldsymbol{H}$ and the vectors $\boldsymbol{X}$ and $\boldsymbol{\Lambda}$ are defined as follows.

$$\boldsymbol{H} = \begin{pmatrix} h_{11} & h_{12} & \dots & h_{1N} \\ h_{21} & h_{22} & \dots & h_{2N} \\ \vdots & \vdots & \ddots & \vdots \\ h_{N1} & h_{N2} & \dots & h_{NN} \end{pmatrix}. \tag{11}$$

$$\boldsymbol{\Lambda} = \begin{pmatrix} \lambda_1 \\ \lambda_2 \\ \vdots \\ \lambda_N \end{pmatrix}. \tag{12}$$

[DOI: 10.1299/mej.22-00140]

$$\boldsymbol{X} = \begin{pmatrix} \chi_1 \\ \chi_2 \\ \vdots \\ \chi_N \end{pmatrix}. \tag{13}$$

$$h_{ij} = w_1 \frac{\int_T D_i D_j d\Omega}{\int_T d\Omega} + w_2 \frac{\int_{\bar{T}} D_i D_j d\Omega}{\int_{\bar{T}} d\Omega} + w_3 \frac{\int_O D_i D_j d\Omega}{\int_O d\Omega}. \tag{14}$$

$$\lambda_i = -2w_1 \frac{\int_T D_i d\Omega}{\int_T d\Omega}. \tag{15}$$

Since χ_i corresponds to the number of particles delivered to each spot, it must be 0 or a positive value at every spot. Finally, the optimization problem is represented as follows.

$$\begin{aligned} &\text{minimize} \quad f, \ \text{with respect to } \chi_i \\ &\text{subject to } \chi_i \geq 0, \quad \text{for} \quad i = 1, 2, ..., N. \end{aligned} \tag{16}$$

Strictly speaking, this should be an integer problem because χ_i is the number of particles. However, we treat it as a real number because the number of particles per spot should be typically at the order of 10^4 or more while the requirement of dose accuracy is around 1%, thus a fraction of χ_i less than one is negligible. Since the objective function f is a quadratic form of χ_i as shown in Eq. (10), this optimization problem is solved with a quadratic programming approach. We use an interior-point algorithm provided by MATLAB, which is suitable to the convex optimization problem as Eq. (16)

2.5. Spot layout optimization

2.5.1. Method of single-remotion

Figure 5 shows a basic flowchart of the proposed method. In this algorithm, only a single spot is simultaneously removed per iteration. A large number of spots are at first placed densely in each layer of the target as the initial state. Then, the particle number optimization process and the spot removing process are alternately repeated and the number of spots decreases step by step. In the spot removing process, the spot with the smallest number of particles is selected as the first candidate to be removed. After one spot is removed, the particle number optimization for the remaining spots is performed and the objective function f is evaluated. If f value exceeds the tolerance level f^*, the removed spot is restored and then the next candidate spot is removed.

The algorithm proceeds by the following steps.

Step 1. $\boldsymbol{X}$ is optimized with the initial spot positions and the initial value of the objective function f is calculated. The tolerance level f^* is set. The value k is set to be 1.

Step 2. The spot with the k-th smallest value of $\boldsymbol{X}$ is removed.

Step 3. $\boldsymbol{X}$ is optimized again with the new spot layout and the objective function f is calculated.

Step 4. When $f \leq f^*$, reset $k = 1$ and return to Step 2. When $f > f^*$, the removed spot is restored and k is incremented as $k = k + 1$. Return to Step 2.

Step 5. The iteration is terminated when k exceeds the number of remaining spots.

In this study, the tolerance level f^* of the objective function is set as 1.3 times the f value at the initial state. At the initial state spots are located dense enough and the dose distribution is considered to be almost ideal. The value 1.3 indicates the level of deterioration from the ideal dose distribution. So this value should be set as small as possible while avoiding an accidental stop of the optimization process caused by a negligible small uplift during the spot elimination steps. We empirically determine this value as 1.3 in which the final dose distribution keeps still acceptable quality enough. Actually, because of the rapid increase of the f value at the near-final steps in the optimization iterations, which is shown later in the section 3.3, the termination timing of the optimization process is considered to be less sensitive to the setting of f^*

[DOI: 10.1299/mej.22-00140]

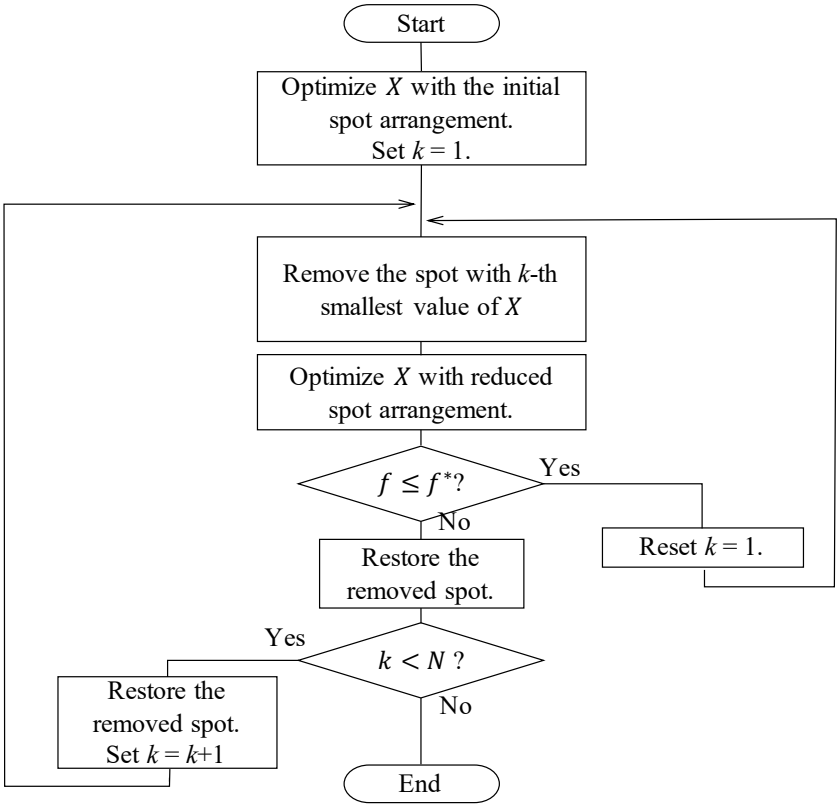

Fig. 5 Flowchart of the algorithm with the method of single-remotion.

2.5.2. Method of multiple-remotion

In a three-dimensional case, the number of spots at the initial state and the number of spots to be removed through optimization is expected to be significantly larger compared with a two-dimensional case, and that leads to a long computation time. On the other hand, in typical particle therapy facilities, new patients come almost every day and the staff must make patient-specific treatment planning on a daily basis. Therefore, a faster optimization process for the spot layout is desired in particle beam therapy. In the proposed method, most of the computation time are spent for the process to create the matrix $\boldsymbol{H}$ in Eq. (10) and to solve the quadratic problem in Eq. (16). Since the quadratic problem is repeatedly solved every time the spot is removed, reducing the number of steps of spot remotion is significantly effective to reduce the computation time.

Figure 6 shows the flowchart of our proposal for an improved method where multiple spots are simultaneously removed to speed up the optimization process. n_r stands for the number of spots to be removed per iteration. After the optimization of χ_i, the spots with the 1st, 2nd, $\cdots$, n_r-th minimum number of particles are removed and the optimization of χ_i with the remaining spots is carried out again. If f value exceeds f^*, the spot remotion is canceled and the next spots with the $n_r + 1$-th, $n_r + 2$-th, $\cdots$, $2n_r$-th minimum number of particles are removed, and then the process continues similarly. When there is no set of n_r continuous spots to be removed without violating f value, the n_r is decreased to the half value. Here, fractions less than 1 are rounded down. Finally, the optimization process is terminated when $n_r = 1$ and there is no single spot to be removed without violating f value.

2.6. Target geometries and parameter setting

2.6.1. Two-dimensional targets

In order to evaluate the effectiveness of the proposed method, we set several test cases on both two-dimensional and three-dimensional bases. Figure 7 shows the test cases for the two-dimensional target: (a) is a square target of 50 mm $\times$ 50 mm, (b) is a circular target with a radius of 30 mm, (c) is a concave target where a 30 mm $\times$ 30 mm square region is cut out from a 50 mm $\times$ 50 mm square, and (d) is a square target of 50 mm $\times$ 50 mm with a circular hole with a radius of 15 mm. The beam size σ is set to be 4 mm. The algorithm of single spot remotion, which is shown in Fig. 5, is applied to each target. With every target, the optimized spot layout is compared to a lattice pattern with a similar number of spots. No OAR is set in two-dimensional cases.

[DOI: 10.1299/mej.22-00140]

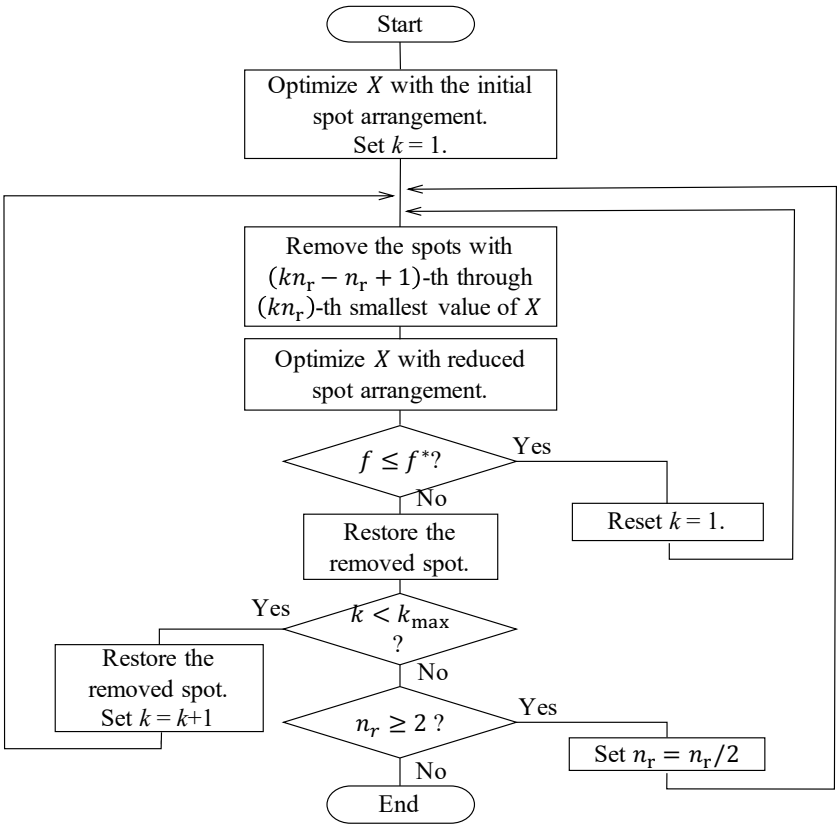

Fig. 6 Flowchart of the algorithm with the method of multiple-remotion.

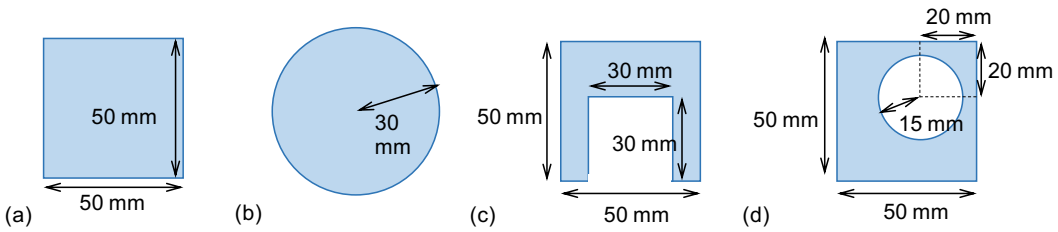

Fig. 7 Geometries of the two-dimensional targets with the shapes of (a) square, (b) circle, (c) concave, and (d) square with a hole

2.6.2. Three-dimensional targets

We also consider a three-dimensional spherical target as shown in Fig. 8. In order to test the effectiveness of the proposed algorithm taking advantage of the Bragg-peak of the particle beam in the depth direction, an OAR is placed very close to the target. The target has a spherical shape with the radius of 30 mm and a center depth of 90 mm. A hollow hemisphere-shaped OAR is located as surrounding the half of the target at the opposite side from the beam direction with 8 mm spacing from the target surface. We set this target geometry because of the following reasons.

- The spherical shape of the target is one of the typical assumption in particle beam therapy, as shown in the prior research, for example, Futami et al. (1999)
- The OAR dose not usually exist at the upstream of the target along the particle beam trajectory, because there is a degree of freedom in deciding the beam irradiation angle and such angles are not selected.
- Filling all the region surrounding the rear half of the target with the OAR should be one of the most difficult setting in sparing the OAR from unnecessary dose.

[DOI: 10.1299/mej.22-00140]

2.6.3. The setting of parameters

For two-dimensional cases, we set the weighting factors as $w_1 = 0.99$ and $w_2 = 0.01$ in the objective function in Eq. (4). For three-dimensional cases, we set $w_1 = 0.950$, $w_2 = 0.003$, and $w_3 = 0.047$. The maximum dose value outside the target is more than half of D_{obj} because of the so-called penumbra structure (Myers et al., 2019), which is the dose drop around the target edge, with the width of typically around 10 millimeter. On the other hand, the dose fluctuation in the target is less than 10 percent of D_{obj}. Since f_1, f_2 and f_3 have a dimension of square of the dose, f_2 and f_3 often have one or two order larger values in a decimal digit compared with f_1. In order to correct the balance and to put closer order of penalty on each objective function, the value of w_1 should be larger than w_2 and w_3. Besides, in three-dimensional cases, w_3 is set to be larger than w_2 because the OAR dose should be reduced with higher priority than a general volume outside the target. The balance among w_1, w_2 and w_3 can be arranged case by case, considering the importance of the requirements of each corresponding objective function. As the initial state in the spot layout optimization process, the spots are located in the lattice layout with a spacing of 2 mm, which corresponds to 0.5σ, both along the x and y directions in two-dimensional targets and in every layer in three-dimensional target. The initial spots are located not only inside the target but also outside the target where the distance from the target boundary is within a margin of 1σ. With the three-dimensional target, the depth of layers is set with a spacing of 4 mm. For every cases in two-dimensional and three-dimensional targets, we set $D_{obj} = 1$. Two-dimensional and three-dimensional dose distributions are calculated with the grid size of 2 mm × 2 mm and 2 mm × 2 mm × 2 mm, respectively.

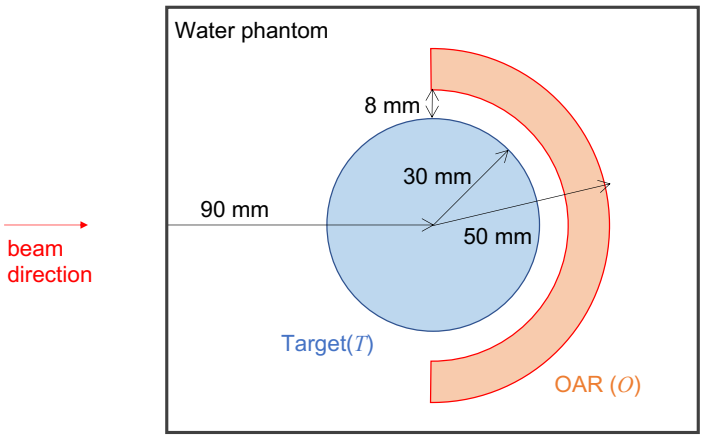

Fig. 8 Geometry of the three-dimensional spherical target

3. Results and Discussions

3.1. Two-dimensional cases

Figure 9 shows the initial states of spot locations for two-dimensional targets (a), (b), (c), and (d). Figure 10 shows the optimized spot layouts for each target. Here, the blue small circles and red solid lines stand for the spot locations and the target contours, respectively. The numbers of spots at the optimized solutions were 76, 84, 54, and 55 for the targets (a), (b), (c), and (d), respectively. On the other hand, we also tested the lattice spot patterns which have a similar number of spots to the optimized ones as shown in Fig. 11. In the optimized spot layouts, more spots were located on the contour of the target, compared with those in the lattice layout. Figure 12 shows the dose distribution with the optimized spot layouts and Fig. 13 shows the dose distribution with the lattice spot layouts for targets (a), (b), (c), and (d). A similar dose distribution which matches the target contour was confirmed for each shape of target. Table 1 shows the comparison of the number of spots and values of the objective function between the optimized spot layout and the lattice spot layout with each target. With every target, the total objective function f with the optimized spot layout was smaller than that with the lattice spot layout. With targets (a) and (b), the objective function f_1, which corresponds to the dose uniformity in the target, with the optimized spot layout was larger than that with the lattice spot layout, while the objective function f_2, which corresponds to the unnecessary dose outside the target, with the optimized spot layout was smaller than that with the lattice spot layout. With targets (c) and (d), on the other hand, both f_1 and f_2 with the optimized spot layout were smaller than those with the lattice spot layout. We can conclude that the proposed method is effective especially in reducing the unnecessary dose outside the target by adjusting the spot locations close to the target contour. Furthermore, these results imply that the proposed method is also effective in forming homogeneous dose distribution in the target when the target contour shape is complicated, as in targets (c) and (d).

[DOI: 10.1299/mej.22-00140]

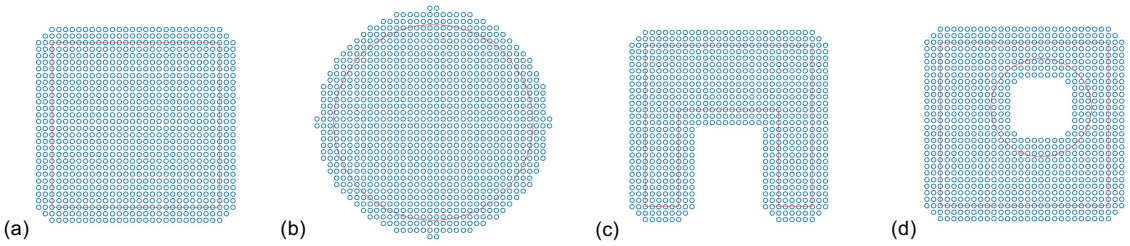

Fig. 9 Initial state of spot locations with two-dimensional targets.

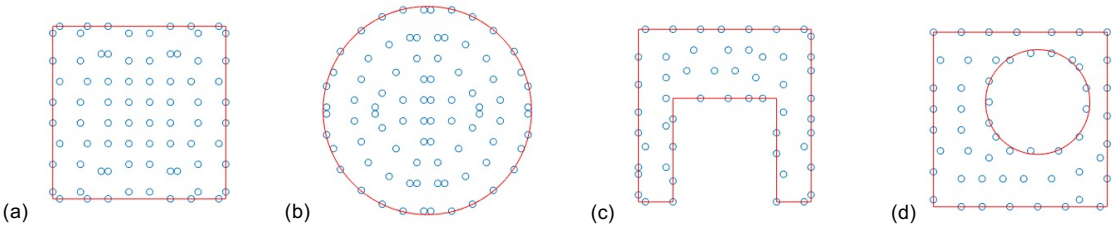

Fig. 10 Optimized spot layout with two-dimensional targets.

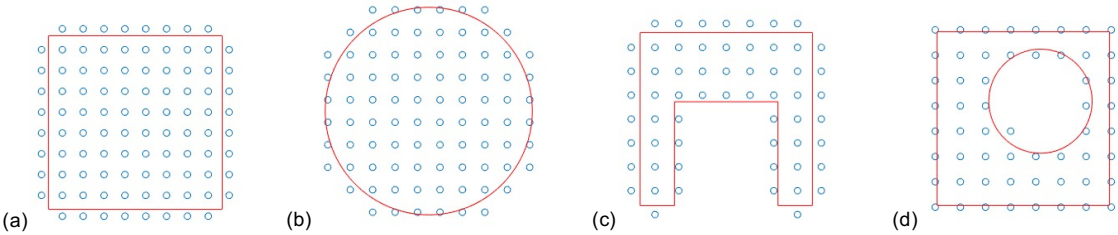

Fig. 11 Lattice spot layout with two-dimensional targets.

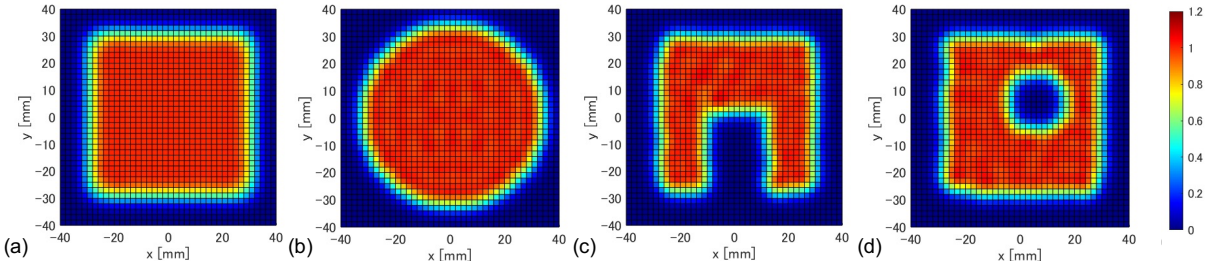

Fig. 12 Dose distribution for the optimized spot layout with two-dimensional targets.

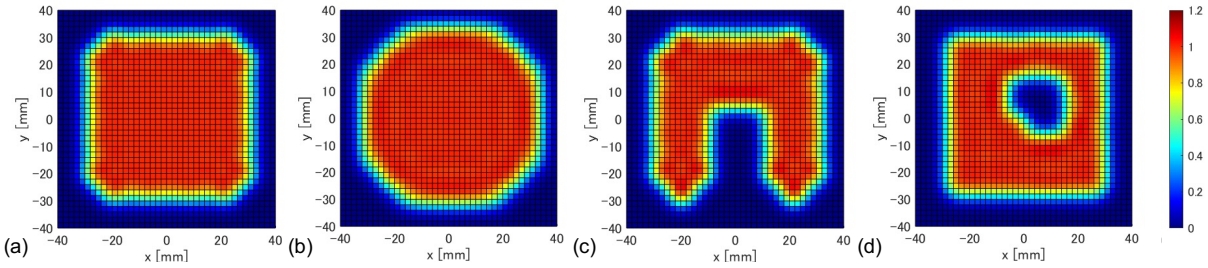

Fig. 13 Dose distribution for the lattice spot layout with two-dimensional targets.

3.2. Three-dimensional case

Figures 14 (a) and (b) show the optimized spot layouts with the proposed method of single-remotion and that with the method of multiple-remotion, respectively. With the method of multiple-remotion, the initial value of n_r, the number of spots to be simultaneously removed per iteration, was set to be 5. On the other hand, Fig. 14 (c) shows the lattice spot layout where the spot spacing was adjusted so that the number of spots became similar to those in the optimized

[DOI: 10.1299/mej.22-00140]

Table 1 Number of spots and value of the objective functions with optimized and lattice spot layouts for the two-dimensional targets.

Target	Spot layout	Number of spots	f ($\times 10^{-3}$)	f_1 ($\times 10^{-4}$)	f_2 ($\times 10^{-2}$)
(a)	Optimized	76	0.93	3.49	5.88
	Lattice	96	1.03	0.97	9.36
(b)	Optimized	84	0.95	2.93	6.57
	Lattice	88	1.04	2.12	8.12
(c)	Optimized	54	1.20	4.02	8.04
	Lattice	60	1.64	4.91	11.5
(d)	Optimized	55	1.33	4.24	9.11
	Lattice	56	1.52	5.34	9.95

layouts. The numbers of spots were 688, 652 and 724 in the spot layouts which were optimized with the methods of single-remotion, multiple-remotion and the lattice layout, respectively. In both optimized spot layouts in Figs. 14 (a) and (b), many spots were located on the contour of the target in each layer, similar to the two-dimensional results shown in Fig. 10. Figures 15 (a) and (b) show the dose distributions in the xz cross-sectional plane with the optimized spot layout for the methods of single-remotion and multiple-remotion, respectively. Here, the white dashed lines show the target contours. On the other hand, Fig. 15 (c) shows the dose distribution with the lattice spot layout. The envelope of the dose distribution around the target edge shows mismatches to the circular shaped contour, while the dose distribution with the optimized spot layout shows a smoother dose distribution conformal to the target as in Figs. 15 (a) and (b). Table 2 shows the comparison of the number of spots and values of the objective function among the optimized spot layouts and the lattice spot layout. Each of the objective functions f, f_1, f_2, and f_3 shows quite similar values in both optimized spot layouts. The objective function f with both optimized spot layouts was reduced to almost half of that with the lattice spot layout. Both f_1 and f_3, which correspond to the dose uniformity in the target and the unnecessary dose to the OAR behind the target, respectively, were smaller with the optimized spot layouts compared to those with the lattice spot layout. The second term f_2, which corresponds to the unnecessary dose outside the target, was almost the same value in every spot layout. This is because the largest contribution to f_2 is the dose in the front region of the target, which is the upstream of the beam trajectory and inevitable to be irradiated regardless of the spot layout. From this result, we consider that the proposed method is effective especially in avoiding an unnecessary dose to the OAR near the target while keeping the dose homogeneity within the target.

3.3. Effectiveness of multiple-remotion method

Figure 16 shows the history of changes in the objective function f through iterations with each method of single-remotion and multiple-remotion. With the method of multiple-remotion, the cases in which the initial n_r values were 5, 10, 20, 40 were compared. The horizontal axis is the total number of removed spots from the initial state through the optimization process. With every case, f value was almost unchanged at the beginning of the optimization process and suddenly increased toward the end of the optimization process. That is because the spots removed at the early phase in the process have very small contributions, while every spot has a certain contribution to form the acceptable dose distribution at the final phase. With the cases of multiple-remotion with $n_r = 5$ and $n_r = 10$, the increase of f came at similar timings to that of single-remotion. On the other hand, with the cases of multiple-remotion with $n_r = 20$ and $n_r = 40$, the increase of f came at earlier timings than that of single-remotion and also multiple-remotion with $n_r = 5$ and $n_r = 10$. Table 3 summarizes the comparison of the initial/final values of the number of spot and the objective function f, and the total computation time. Through this study, we used a Windows computer with Intel Core-i5 1145G7 CPU (2.6GHz) and 16GB RAM. It is shown that larger value of n_r could make computation time much shorter and there is a trade-off between the solution quality and the computation time in the setting of n_r value. For our problem setting of the three-dimensional target, we consider it is appropriate to set n_r value around 5 to 10, because it can accelerate the optimization process without any significant deterioration in the quality of obtained spot layout.

3.4. Initial state dependence

The computation time of the optimization process depends not only on n_r values but also on the number of spots at the initial state. In order to clarify this dependency, the computation time and the objective function was investigated by varying the spot spacing of the initial lattice from 1.6 mm to 6.0 mm along both x and y direction. Figure 17 (a) shows the relationship between the f values and the number of spots at the initial spots depending on the initial spot spacing. Larger

[DOI: 10.1299/mej.22-00140]

Fig. 14 Spot locations in each layer with (a) optimized spot layout with the method of single-remotion, (b) optimized spot layout with the method of multiple-remotion, and (c) lattice spot layout with the three-dimensional target.

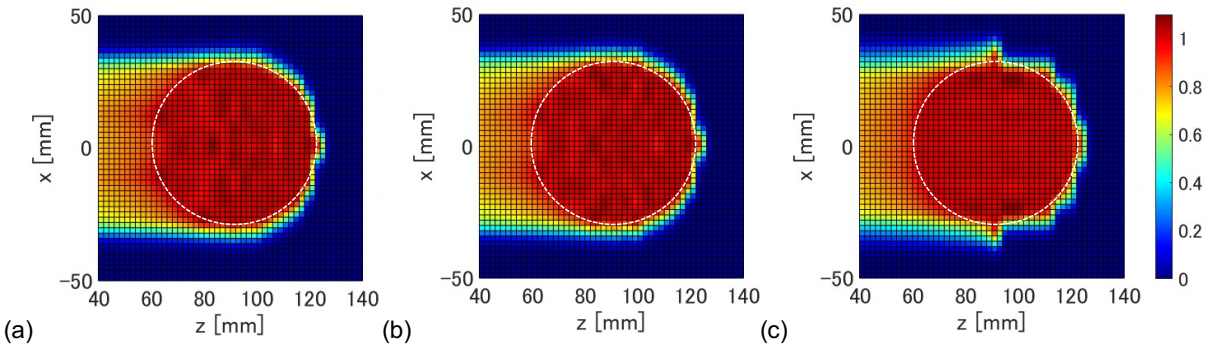

Fig. 15 Dose distribution at the xz cross-sectional plane with (a) optimized spot layout with the method of single-remotion, (b) optimized spot layout with the method of multiple-remotion, and (c) lattice spot layout with the three-dimensional target.

Table 2 Number of spots and value of objective functions with optimized and lattice spot layouts for the three-dimensional target.

Spot layout	Number of spots	f ($\times 10^{-4}$)	f_1 ($\times 10^{-4}$)	f_2 ($\times 10^{-2}$)	f_3 ($\times 10^{-3}$)
Optimized (single-remotion)	688	4.64	1.54	9.55	0.66
Optimized (multiple-remotion)	652	4.64	1.51	9.61	0.67
Lattice	724	9.01	5.76	9.51	1.45

[DOI: 10.1299/mej.22-00140]

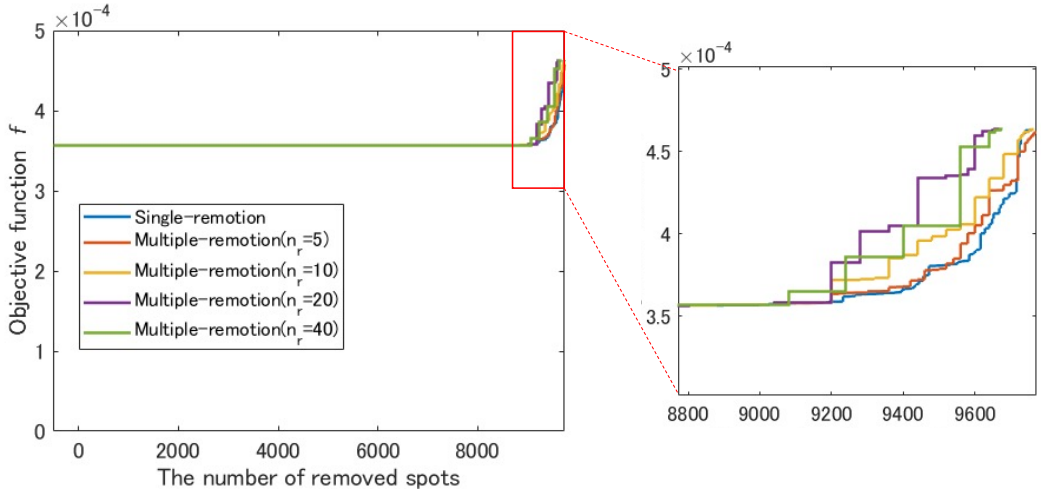

Fig. 16 Changes in the objective function f in the optimization processes with the method of single-remotion, the method of multiple-remotion. The right side figure shows the enlarged view.

Table 3 The number of spots and the objective function at the initial and the final state, and the computation time, with single-remotion and multiple-remotion methods with initial n_r value of 5, 10, 20 and 40.

Initial value of n_r	Initial number of spots	Initial value of f ($\times 10^{-4}$)	Final number of spots	Final value of f ($\times 10^{-4}$)	Computation time [sec]
1	11128	3,57	688	4.64	36073
5	11128	3,57	652	4.64	7461
10	11128	3,57	684	4.64	3697
20	11128	3,57	776	4.64	2094
40	11128	3,57	772	4.64	1078

value of the initial spot spacing leaded to larger value of f and smaller number of spots. Changes in the objective function f through the optimization processes are shown in Fig. 17 (b). The horizontal axis is the total number of remained spots at each step. For all of the cases, the method of multiple-remotion were applied and the initial n_r were set to be 10. Table 4 shows the summary of the initial and the final values of the number of spots and the objective function f, and the total computation time. There was a trend that larger value of the initial spot spacing resulted in larger value of f not only at the initial state but also at the final state. The final number of spots were similar values around 700 for all the cases while there was a small fluctuation depending on the initial spot spacing. Regarding f at the final state, the cases with the initial spot spacing of 1.6 mm, 2.0 mm, 2.4 mm, 3.0 mm, 4.0 mm reached similar values. On the other hand, the final f values with the initial spot spacing of 5.0 mm and 6.0 mm were apparently larger than those with 1.6-4.0 mm. The computation time was obviously shorter when the initial spot spacing was larger. From these results, we conclude that the initial spot spacing can be determined by considering the trade-off between the computation time and the objective value, but it should be at most 4.0 mm which corresponds to just the same value to the beam spot size σ.

4. Conclusion

In this paper, we proposed an optimization method for the spot position layout to determine the scanning magnet operation in particle therapy. We achieved the following:

(1) We formulated the objective function to evaluate the spot layout and the dose distribution considering the dose homogeneity within the target and the dose reduction outside the target.

(2) The spot layout optimization algorithm was constructed, where the spots were densely located at the initial state and removed step by step through iterations based on the contribution of each spot.

(3) The algorithm was confirmed and the effectiveness was shown by examples of the two-dimensional and three-dimensional targets. With the optimized spot layout, the objective functions showed better values than those with the conventional lattice spot layout with similar numbers of spots. We also found that many spots were located on the contour of the target with the optimized spot layout.

(4) Furthermore, we confirmed the method of multiple-remotion could effectively accelerate the optimization process with very small degradation in the dose quality in the solution.

[DOI: 10.1299/mej.22-00140]

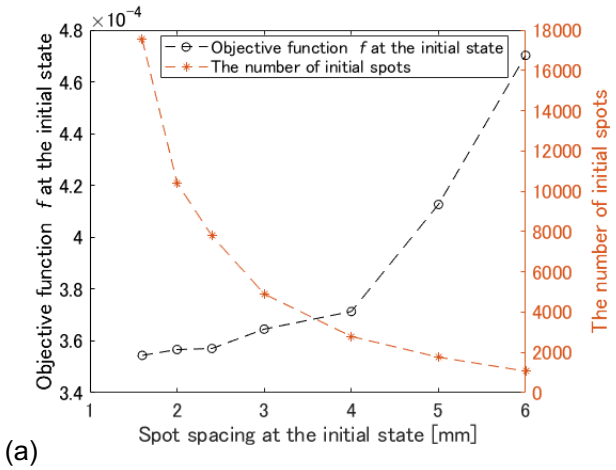

(a)

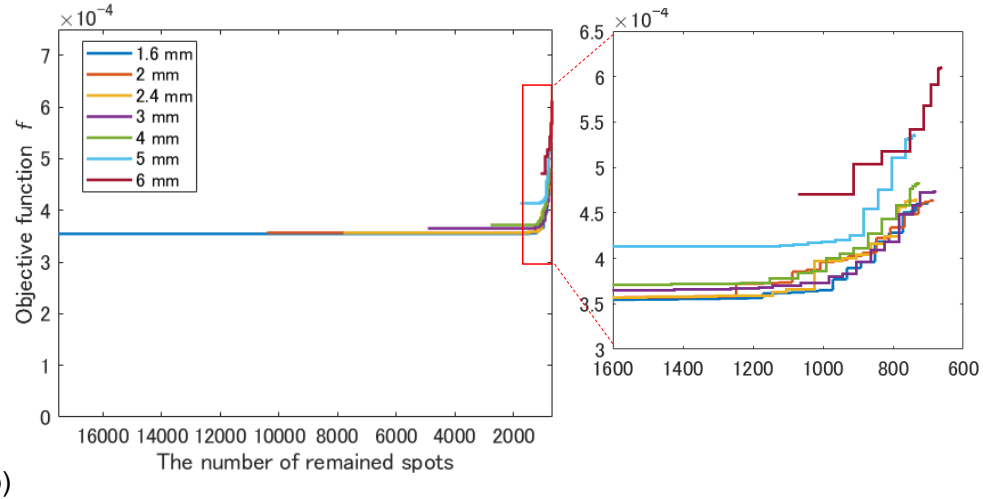

(b)

Fig. 17 (a) The objective function f and the number of spots at the initial state depending on the initial spot spacing. (b) Changes in the objective function f in the optimization processes with various values of the initial spot spacing, with the method of multiple-remotion with $n_r = 10$. The right side figure shows the enlarged view.

Table 4 The number of spots and the objective function at the initial and the final state, and the computation time, among various initial state settings. For all the cases initial value of n_r were 10.

Initial spot spacing [mm]	Initial number of spots	Initial value of f ($\times 10^{-4}$)	Final number of spots	Final value of f ($\times 10^{-4}$)	Computation time [sec]
1.6	17572	3.54	700	4.61	12564
2.0	11128	3.57	684	4.64	3697
2.4	7824	3.57	732	4.64	1413
3.0	4904	3.65	676	4.73	402
4.0	2832	3.71	724	4.83	162
5.0	1804	4.13	736	5.36	110
6.0	1232	4.70	664	6.11	93

References

Akagi, T., Aso, T., Iwai, G., Kimura, A., Kameoka, S., Lee, B. S., Maeda, Y., Matsufuji, N., Nishio, T., Omachi, C., Park, S., Sasaki, T., Toshito, T., Takase, W., Yamashita, T. and Watase, Y., Geant4-based particle therapy simulation framework for verification of dose distributions in proton therapy facilities, Progress in Nuclear Science and Technology, Vol. 4 (2014), pp. 896-900. DOI:10.15669/pnst.4.896

Fukushima, H., Kamada, Y. and Hagiwara, I., Optimum Engine Mounting Layout using MPOD, Transactions of the Japan Society of Mechanical Engineers Series C. Vol. 70, No. 689 (2004), pp. 54-61. (in Japanese) DOI:10.1299/kikaic.70.54.

[DOI: 10.1299/mej.22-00140]

Futami, Y., Kanai, T., Fujita, M., Tomura, H., Higashi, A., Matsufuji, M., Miyahara, N., Endo, M., Kawachi, K., Broad-beam three-dimensional irradiation system for heavy-ion radiotherapy at HIMAC, Nuclear Instruments and Methods in Physics Research A, Vol. 430 (1999), pp. 143-153. DOI:10.1016/S0168-9002(99)00194-1

Kanai, T., Kawachi, K., Matsuzawa, H. and Inada, T., Three-dimensional beam scanning for proton therapy. Nuclear Instruments and Methods in Physics Research. Vol. 214 (1983), pp. 491-496. DOI:10.1016/0167-5087(83)90621-X.

Kang, J. H., Wilkens, J. J. and Oelfke, U., Demonstration of scan path optimization in proton therapy, Medical Physics. Vol. 34 (2007), pp. 3457-3464. DOI:10.1118/1.2760025

Kraft, G., Tumor therapy with heavy charged particles. Progress in Particle and Nuclear Physics, Vol. 45 (2000), pp. 473-544. DOI:10.1016/S0146-6410(00)00112-5.

Krämer, M., Jäkel, O., Haberer, T., Kraft, G., Schardt, D. and Weber, U. Treatment planning for heavy-ion radiotherapy: physical beam model and dose optimization. Physics in Medicine and Biology, Vol. 45 (2000), pp. 3299-3317.

Loeffler, J. S. and Durante, M., Charged particle therapy-optimization, challenges and future directions, Nature Reviews Clinical Oncology, Vol. 10 (2013, pp. 411-424. DOI:10.1038/nrclinonc.2013.79.

Matsumoto, Y., Tanaka, K. and Nakamura, M., Placement optimization of solar arrays in photovoltaic power generation facility site, Transactions of the Japan Society of Mechanical Engineers, Vol. 87, No. 899 (2021), p.21-00066. (in Japanese) DOI:10.1299/transjsme.21-00066.

Meier, G., Leiser, D., Besson, R., Mayor, A., Safai, S., Weber, D. C. and Lomax, A. J., Contour scanning for penumbra improvement in pencil beam scanned proton therapy. Physics and Medicine and Biology, Vol. 62 (2017), pp. 2398–2416. DOI:10.1088/1361-6560/aa5dde

Miao, C. H., Liu, M., Yin, C. X. and Zhao, Z. T., Precise magnetic field control of the scanning magnets for the APTRON beam delivery system. Nuclear Science and Techniques, Vol. 28 (2017), 172. DOI:10.1007/s41365-017-0324-6.

Myers, S., Degiovanni, A. and Farr, J. B., Future Prospects for Particle Therapy Accelerators. Reviews of Accelerator Science and Technology, Vol. 10, No. 1 (2019), pp. 49-92. DOI:10.1142/S1793626819300056

Nishiura, Y., Hirata, K., Ohya, K., Sakaidani, Y. and Niguchi, N., Optimization of the Stator Pole Arrangement of 3-Degree of Freedom Spherical Actuator Using Genetic Algorithm. Journal of the Japan Society of Applied Electromagnetics and Mechanics, Vol. 23, No. 2 (2015), pp.332-337. (in Japanese) DOI:10.14243/jsaem.23.332.

Pedroni, E., Bacher, R., Blattmann, H., Böhringer T., Coray A., Lomax A., Lin S., Munkel G., Scheib S., Schneider U. and Tourovsky, A., The 200-MeV proton therapy project at the Paul Scherrer Institute: conceptual design and practical realization. Medical Physics, Vol. 22 (1995), pp. 37-53. DOI:10.1118/1.597522.

Wu, C., Pu, Y. H., Zhang X., GPU-accelerated scanning path optimization in particle cancer therapy, Nuclear Science and Techniques, Vol. 30 (2019), 56. DOI:10.1007/s41365-019-0582-6

Yamaki, Y., Sato, Y., Izui, K., Yamada, T., Nishiwaki, S., Hirai, Y. and Tabata, O., A heuristic approach for actuator layout designs in deformable mirror devices based on current value optimization, Structural Multidisciplinary Optimization, Vol. 58 (2018), pp. 1243-1254. DOI:10.1007/s00158-018-1968-5.

[DOI: 10.1299/mej.22-00140]